Theory of evanescent mode atomic mirrors with a metallic layer

C. R. Bennett,[1] J. B. Kirk,[2] and M. Babiker[1]
[1]*Department of Physics, University of York, Heslington, York YO10 5DD, United Kingdom*
[2]*Department of Physics, University of Essex, Colchester, Essex CO4 3SQ, United Kingdom*
(Received 8 June 2000; published 13 February 2001)

Dielectric atomic mirrors are considered in which the repulsive force field owes its existence to an evanescent mode in the presence of a metallic capping layer. The theory of such an atomic mirror is constructed, assuming a finite thickness of the metallic layer with a finite plasma frequency and adopting the field-dipole orientation picture. The Rabi frequency together with the reflectivity for the light incident from within the substrate are evaluated, and their variations with the type of metal and layer thickness analyzed as useful indicators of the effectiveness of the system as an atomic mirror. A number of interesting features are pointed out, including a desirable enhancement. Solutions of the equation of motion for a given atom, subject to given initial conditions, lead to trajectories exhibiting reflection. The leading force fields controlling the dynamics include the average dipole image force plus the average light-induced forces due to the evanescent field. The parameters used to compute the trajectories are similar to those in recent experiments in which Rb atoms incident on a silver film deposited on a glass substrate have been shown to experience enhanced mirror action. The factors controlling the enhancement in general are pointed out and discussed.

DOI: 10.1103/PhysRevA.63.033405 PACS number(s): 42.50.Vk, 03.75.Be, 42.87.Bg

I. INTRODUCTION

It was Cooke and Hill [1] who first put forward the suggestion that light-induced forces in the vicinity of a planar surface can be used to reflect neutral atoms. Their suggestion paved the way towards the realization of an atomic mirror although, to date, the standardization of the atomic mirror as a routine tool is yet to be achieved. Currently the study of atomic mirrors forms an important branch of the main stream of atom optics [2,3], with atomic mirrors continuing to receive attention by both theory and experiment dealing with various mechanisms for mirror action [4–19].

Particular kinds of atomic mirrors which continue to receive much attention are variants of the evanescent mode atomic mirror [1–3,15,18,19]. The basic principle still applies, namely that the average repulsive force field responsible for the reflection process is set up by an evanescent light field which occurs when light incident from within a dielectric substrate is internally reflected at the surface. The factors which limit the performance of such mirrors stem mainly from heating effects and also from fluctuations which become less severe at low intensities. Provided that the light intensity is not too low and its frequency is suitably blue-detuned from the atomic resonance frequency, the average dipole force field set up by this evanescent component may overcome the attractive van der Waals force between the atom and the mirror surface creating an overall repulsive barrier for the approaching atom. The higher the barrier, the more effective the system is as an atomic mirror. A reduction of fluctuation effects at low intensities was the main reason for investigations to construct an atomic mirror operating at low intensities. This requires the modification of the main mirror ingredients to achieve an enhancement at low intensities. Since the van der Waals force is not amenable to modification in the basic kind of evanescent mode atomic mirror, control of the effective barrier to achieve an enhanced mirror action can only be done by controlling the properties of the evanescent field. A particular method for achieving enhancement is by the addition of a metallic capping layer.

That enhancement can indeed be achieved has been demonstrated experimentally by Feron *et al.* [18] and Esslinger *et al.* [19] using a metallic film deposited on the surface of a planar dielectric. However, as far as we know, no primarily analytical theory has been constructed which describes the mirror action and the nature of the enhancement as a direct consequence of the metallic layer and which also facilitates the derivation of atomic trajectories. The purpose of this paper is to construct such a theory. In order to perform a quantitative analysis of such an atomic mirror, we need to incorporate a number of ingredients. First, full account should be taken of the finite thickness and finite electron density of the metallic layer together with the metallic conductivity loss, as contained in the imaginary part of the dielectric function. Second, in order to account for the dependence on the incident light intensity, a proper mode normalization in terms of this intensity is needed for the light mode generating the evanscent component. Third, the average attractive potential due to the interaction between the dipole and its image in the presence of the metallic layer should be included in the dynamics. We show here that a theoretical framework incorporating these ingredients leads to the average atomic trajectories, predicting either a reflection of the atom off the surface or a collision with it, in a manner dependent on the chosen set of parameters.

The outline of this paper is as follows. In Sec. II we describe the basic elements comprising the atomic mirror, including a metallic film of a finite thickness. The procedure needed for the specification of the light mode bearing the evanescent component is then described, leading to appropriate field distributions in the three regions of the structure. In Sec. III we derive an expression for the reflectivity of the

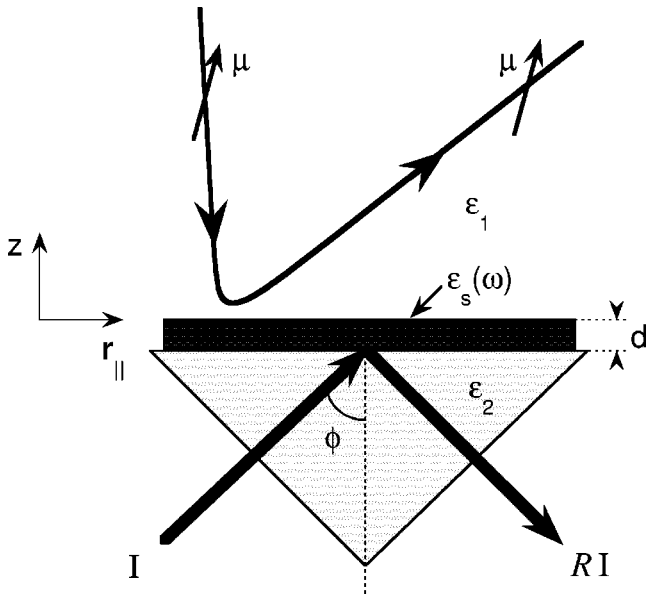

FIG. 1. Schematic arrangement of the elements comprising an evanescent mode atomic mirror with a metallic layer of thickness *d*. The plane of incidence contains the internally reflected light beam as well as a typical atomic trajectory. *I* is the intensity of the light at an angle of incidence ϕ; *R* is the reflectivity of the inner substrate surface; $\boldsymbol{\mu}$ is the electric dipole moment vector, and ϵ_1, ϵ_s, and ϵ_2 are the dielectric functions of the different regions. Here both the atom and the light are asumed to be initially propagating on the same side of the vertical.

inner substrate surface. We also define the Rabi frequency associated with the evanescent light at the outer film surface using the field-dipole orientation picture. We explain how the variations of these properties with the angle of incidence and layer thickness help to provide insight into the nature of the enhancement. Section IV deals with the dynamics of Rb atoms and derives trajectories demonstrating the mirror action, assuming a typical mirror setup. Section V contains the main conclusions and provides further comments, including a brief discussion of the thin film limit of our theory.

II. EVANESCENT FIELD

The basic components of the atomic mirror are shown in Fig. 1. Here a metallic layer of thickness *d* is deposited on the planar surface of a glass prism (forming the dielectric substrate). Light of frequency ω is incident at an angle ϕ and is propagating on the left-hand side of the vertical axis within the glass prism. This light is internally reflected at the inner interface between the prism and the metallic layer, and partially leaks into the metallic layer. The light within the metallic layer subsequently generates evanescent light in the vacuum region of the layer system. A neutral atom possessing a transition frequency $\omega_0 < \omega$ moving in the plane of incidence towards the outer surface of the structure would be subject to an average repulsive dipole force plus an average light pressure force, both owing their existence to the presence of the evanescent field. The atom would also be subject to an average dipole image force. It is the combined influence of these average forces that is responsible for the mirror action.

In order to determine the average force fields due to the light we must evaluate the amplitude of the evanescent electric field. This is done by applying the standard electromagnetic boundary conditions at the interfaces and by normalizing the incident field. The electric field vector in the mirror structure can be written in quantized form as follows:

$$\mathbf{E}(\mathbf{k}_\parallel,\mathbf{r},t)=\boldsymbol{\mathcal{E}}(\mathbf{k}_\parallel,z)e^{i(\mathbf{k}_\parallel\cdot\mathbf{r}_\parallel-\omega t)}a+\text{H.c.}, \tag{1}$$

where *a* is a mode annihilation operator, H.c. stands for the Hermitian conjugate, and $\boldsymbol{\mathcal{E}}(\mathbf{k}_\parallel,z)$ is the electric field distribution within the three regions of the layer system which can be written in the following general form involving field amplitudes *A*, *B*, *C*, *D*, and *G*,

$$\boldsymbol{\mathcal{E}}(\mathbf{k}_\parallel,z<-d)=A\left(1,0,-\frac{k_\parallel}{k_{z2}}\right)e^{ik_{z2}z}+B\left(1,0,\frac{k_\parallel}{k_{z2}}\right)e^{-ik_{z2}z}, \tag{2}$$

$$\boldsymbol{\mathcal{E}}(\mathbf{k}_\parallel,-d<z<0)=C\left(1,0,-i\frac{k_\parallel}{k_{zs}}\right)e^{k_{zs}z}+D\left(1,0,i\frac{k_\parallel}{k_{zs}}\right)e^{-k_{zs}z}, \tag{3}$$

$$\boldsymbol{\mathcal{E}}(\mathbf{k}_\parallel,z>0)=G\left(1,0,i\frac{k_\parallel}{k_{z1}}\right)e^{-k_{z1}z}. \tag{4}$$

Here $\mathbf{k}_\parallel$ is the wave vector parallel to the surface. Its magnitude $k_\parallel$ is given by $c^2k_\parallel^2=\omega^2\epsilon_2\sin^2\phi$ where ϕ is the angle of incidence. The three quantities between the brackets in each of Eqs. (2)–(4) stand for the vector components parallel to $\mathbf{k}_\parallel$, perpendicular to it on the surface plane and along the *z* direction, respectively. The notation is such that parameters associated with the substrate are labeled by subscript 2, those associated with the metallic layer are labeled by subscript *s*, while for the outer region (vacuum) the label is 1. The dielectric functions ϵ_2 and ϵ_s are, in general, frequency dependent, while we assume that $\epsilon_1=1$, as appropriate for vacuum. The real wave vectors k_{z1} and k_{z2} are associated with field variations normal to the interfaces in regions 1 and 2, respectively, and are defined by

$$k_{z1}^2=k_\parallel^2-\frac{\epsilon_1\omega^2}{c^2}>0, \quad k_{z2}^2=\frac{\epsilon_2\omega^2}{c^2}-k_\parallel^2>0, \tag{5}$$

while k_{zs}, which is in general complex, is associated with field variations normal to the interface in the metallic layer and is defined by

$$k_{zs}^2=k_\parallel^2-\frac{\epsilon_s\omega^2}{c^2}. \tag{6}$$

The dielectric function ϵ_s of the metallic layer is given by

$$\epsilon_s = 1 - \frac{\omega_p^2}{\omega(\omega + i\gamma)}, \tag{7}$$

where ω_p is the plasma frequency of the metal and is defined as $\omega_p^2 = n_0 e^2/m^* \epsilon_0$, with m^* and e the electronic effective mass and charge, respectively, and n_0 is the volume electron density of the metal. In Eq. (7) we have included an imaginary part of the dielectric function in order to account for the metallic plasma loss effects.

Next we apply the standard electromagnetic boundary conditions, namely the continuity of the tangential component of the electric field vector and the continuity of the normal component of the displacement field vector at both interfaces $z=0$ and $z=-d$. Continuity conditions for the tangential electric field vector at $z=0$ and $z=-d$ yield, respectively,

$$C + D = G, \tag{8}$$

$$Ae^{-ik_{z2}d} + Be^{ik_{z2}d} = Ce^{-k_{zs}d} + De^{k_{zs}d}. \tag{9}$$

From the continuity of $\epsilon \mathcal{E}_z$ at $z=0$ and $z=-d$ we have, respectively,

$$\frac{\epsilon_s}{k_{zs}}(D - C) = \frac{\epsilon_1}{k_{z1}} G, \tag{10}$$

$$\frac{\epsilon_2}{k_{z2}}(Be^{ik_{z2}d} - Ae^{-ik_{z2}d}) = i\frac{\epsilon_s}{k_{zs}}(De^{k_{zs}d} - Ce^{-k_{zs}d}). \tag{11}$$

Equations (8)–(11) allow a direct, albeit somewhat laborious, evaluation of the evanescent field amplitude G in terms of the incident field amplitude A. We find

$$G = \frac{2Ae^{-ik_{z2}d}}{\xi}, \tag{12}$$

where ξ is given by

$$\xi = \left(1 - i\frac{k_{z2}\epsilon_1}{k_{z1}\epsilon_2}\right)\cosh(k_{zs}d) + \left(\frac{k_{zs}\epsilon_1}{k_{z1}\epsilon_s} - i\frac{k_{z2}\epsilon_s}{k_{zs}\epsilon_2}\right)\sinh(k_{zs}d). \tag{13}$$

The amplitude A of the incident field is conveniently fixed by canonical methods, treating the incident field as though it is in an infinite bulk. The field Hamiltonian is such that

$$\mathcal{H}_I = \frac{\epsilon_0}{2}\int d\mathbf{r}\left\{\frac{\partial(\epsilon_2\omega)}{\partial\omega}E_I^2 + \frac{1}{\epsilon_0 c^2}H_I^2\right\} = \tfrac{1}{2}\hbar\omega(aa^\dagger + a^\dagger a), \tag{14}$$

where the label I emphasizes the incident part of the electric field in the substrate [proportional to A in Eq. (2)] with $\mathbf{H}_I$ the corresponding magnetic field. The canonical condition Eq. (14) gives straightforwardly

$$A^2 = \frac{\hbar k_{z2}^2 c^2}{V\epsilon_0\epsilon_2\left(\omega\frac{\partial\epsilon_2}{\partial\omega} + 2\epsilon_2\right)\omega}, \tag{15}$$

where V is a large volume of material 2.

III. REFLECTIVITY AND RABI FREQUENCY

The reflectivity of the internal surface at $z=-d$ within the substrate is an important property of the atomic mirror that we shall discuss in some detail. This is defined by the modulus square of the ratio between the reflected and incident amplitudes in Eq. (2)

$$R = \left|\frac{B}{A}\right|^2. \tag{16}$$

The ratio B/A can be evaluated in an analogous manner to that leading to Eq. (12). We find

$$\frac{B}{A} = \frac{e^{-2ik_{z2}d}}{\xi}\left[2\left(\cosh(k_{zs}d) + \frac{k_{zs}\epsilon_1}{k_{z1}\epsilon_s}\sinh(k_{zs}d)\right) - \xi\right], \tag{17}$$

where ξ is given by Eq. (13). We should note that the ratio B/A is, in general, complex, not just because of the exponential factor in Eq. (17) but also by virtue of the finiteness of the imaginary part (proportional to γ) of the dielectric function ϵ_s, as defined in Eq. (7). Also note that in the limit $\gamma = 0$ the reflectivity becomes identically equal to unity, as can be easily verified from Eq. (17)).

The second important property of the atomic mirror is the Rabi frequency Ω_R. This characterizes the interaction of a neutral atom of electric dipole moment $\boldsymbol{\mu}$ approaching the mirror from the vacuum region ($z>0$) and, so, interacting with the evanescent light. The Rabi frequency is defined as

$$\Omega_R = \left|\frac{\alpha\boldsymbol{\mu}\cdot\boldsymbol{\mathcal{E}}(\mathbf{k}_\parallel, z>0)}{\hbar}\right|, \tag{18}$$

where α is a complex amplitude factor such that in the classical electromagnetic field limit we have $a \to \alpha$. In fact $|\alpha|$ is related to the field intensity by the well-known relation [20]

$$|\alpha|^2 = \frac{IV}{\hbar\omega c}. \tag{19}$$

It can be seen from Eq. (4) that the evanescent field possesses two vector components within the plane of incidence. In general, the electric dipole could have an arbitrary orientation relative to the electric field vector. However, once the evanescent field has been set up, the atomic dipole moment aligns itself parallel to and follows the oscillation of the local electric field vector. This field-dipole orientation picture was also implemented to evaluate trajectories in the context of atom guides [21]. The appropriate Rabi frequency in this field-dipole orientation picture is thus given by

$$\hbar\Omega_R(z>0) = |\alpha|\mu\mathcal{E}(z>0), \tag{20}$$

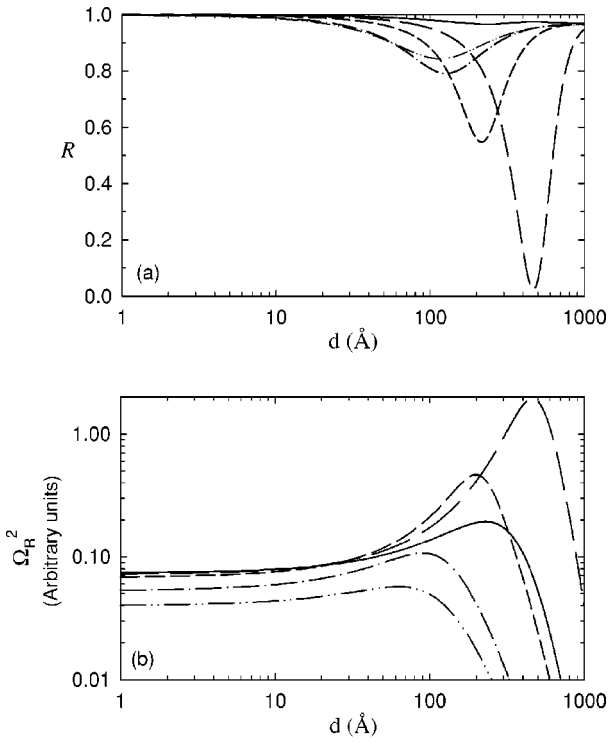

FIG. 2. Variation with the silver layer thickness d of (a) the reflectivity R of the inner surface within the substrate and (b) Ω_R^2, the squared evanescent mode Rabi frequency (in arbitrary units), evaluated at $z=0$. The frequency of the light corresponds to the Rb transition wavelength $\lambda_0=780$ nm and the plasma loss parameter γ is taken to be $\gamma=8.0\times10^{-3}\omega_p^{\text{silver}}$. In both figures the different curves correspond to different angles of incidence: $\phi=41.80°$ (full curve); $\phi=42.20°$ (long dashes); $\phi=43.00°$ (short dashes); $\phi=47.00°$ (dash-dots); and $\phi=52.00°$ (dash-double dots).

where μ and $\mathcal{E}(z>0)$ are the magnitudes of these vectors. Using Eqs. (4), (12), and (15), we have for the square of the Rabi frequency

$$\Omega_R^2(z>0)=\frac{4|\alpha|^2\mu^2k_{z2}^2c^2(1+k_\parallel^2/k_{z1}^2)e^{-2k_{z1}z}}{\hbar V\epsilon_0\epsilon_2\left(\omega\dfrac{\partial\epsilon_2}{\partial\omega}+2\epsilon_2\right)\omega|\xi|^2}. \quad (21)$$

Figure 2(a) displays the variation of the reflectivity, given by Eqs. (16) and (17), in the case of a silver film, with varying thickness d. The parameter γ entering the imaginary part of ϵ_s is taken as $\gamma=8.0\times10^{-3}\omega_p^{\text{silver}}$ [18]. We have also assumed that ϵ_2 does not depend on the frequency and so we set $\partial\epsilon_2/\partial\omega=0$. The different curves in this figure correspond to different values of angle of incidence ϕ, as detailed in the caption to Fig. 2. Figure 2(b) shows the corresponding variation of Ω_R^2 [given by Eq. (21), evaluated at $z=0$] with metallic layer thickness for the same values of ϕ and using the same parameters.

There are a number of features in Fig. 2 which are worthy of note. For a given ϕ the variation of the reflectivity R shown in Fig. 2(a) is initially close to unity, but subsequently exhibits a marked minimum at a well-defined layer width. In fact the positions of these minima correspond closely to those of the maxima of Ω_R^2 in Fig. 2(b). Values of Ω_R^2 at $d=0$ in Fig. 2(b) are appropriate for the case with no metallic layer. As d increases, for a given ϕ, the squared Rabi frequency Ω_R^2 shows a gradual increase up to a point where it subsequently exhibits an enhancement. It is easy to check that the reflectivity minima and the maxima of Ω_R^2 satisfy the condition where $|\xi|^2$ is a minimum. The maximum in Ω_R^2 is followed by a decrease to diminished values at large layer widths. The latter feature is indicative of screening effects when the metallic layer becomes too thick to permit an evanescent field outside. Note the presence of the second term which is proportional to $k_\parallel^2/k_{z1}^2$ in the numerator of Eq. (21). This is the contribution from the z component of the evanescent electric field and since k_{z1} can be very small (when the angle of incidence is close to the total internal reflection angle ϕ_0), this further contributes to the enhancement.

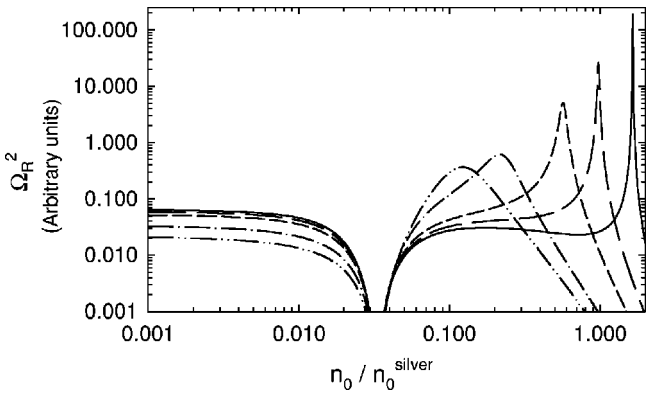

FIG. 3. Variation of Ω_R^2 with electron density n_0 (in units of $n_0^{\text{silver}}=5.57\times10^{28}$ m^{-3}). Here we have set $\gamma=0$ and the curves correspond to $\phi=41.80°$ (full curve); $\phi=42.20°$ (long dashes); $\phi=43.00°$ (short dashes); $\phi=47.00°$ (dash-dots); and $\phi=52.00°$ (dash-double dots). The parameters are such that $\epsilon_2=2.298$, corresponding to an angle of total internal reflection $\phi_0=41.27°$.

Figure 3 displays curves for Ω_R^2 against n_0, the metallic electron density, for a fixed layer thickness $d=59$ nm and where we set $\gamma=0$. As n_0 increases at a fixed ϕ the squared Rabi frequency Ω_R^2 exhibits an initial dip at a value of n_0 corresponding to the plasma resonance at $\omega_p\approx\omega$. This is followed by a resonance at a characteristic density $n_0=n_0^\phi$ and it is seen that the resonance grows as the angle ϕ gets closer to $\phi_0=41.27°$. At ϕ_0 the Rabi frequency becomes very large, with a variation in the form of a delta distribution. In principle, then pronounced repulsion effects would be expected in conditions corresponding to the peak of the Rabi frequency, or the minimum of the reflectivity.

IV. TRAJECTORIES AND MIRROR ACTION

The total average radiation force acting on an atom of transition frequency ω_0 moving in the vacuum region of the layer structure shown in Fig. 1 at velocity $\mathbf{v}$ is given by [21,22]

$$\mathbf{F}(\mathbf{r},\mathbf{v})=2\hbar\left\{\frac{\Gamma\Omega_R^2\mathbf{k}_\parallel-\dfrac{1}{2}\Delta\boldsymbol{\nabla}\Omega_R^2}{\Delta^2+2\Omega_R^2+\Gamma^2}\right\}=\mathbf{F}_s+\mathbf{F}_d, \quad (22)$$

where $\mathbf{F}_s$ corresponds to the first term within the brackets, identified as the average spontaneous force along the wave propagation direction $\mathbf{k}_\parallel$ and $\mathbf{F}_d$ corresponds to the second term, identified as the average dipole force. Δ is the dynamic detuning given by

$$\Delta(\mathbf{v}) = \Delta_0 - \mathbf{k}_\parallel \cdot \mathbf{v}, \tag{23}$$

where $\Delta_0 = \omega - \omega_0$ is the static detuning of the light from the atomic resonance. It is easy to see that $\mathbf{F}_d$ acts as a repulsive force provided that the detuning Δ is positive (blue detuning). Note also that $\mathbf{v}$, the atomic velocity vector, is in the plane of incidence, as in Fig. 1, i.e., it has two components, a z component and a component parallel to $\mathbf{k}_\parallel$.

Besides the radiation forces given by Eq. (22), the atom experiences an attractive force due to the coupling of the dipole to the vacuum fields which are modified (relative to free space) by the layered structure comprising the atomic mirror. For atoms located at distances from the mirror surface smaller than a reduced transition wavelength $\lambda_0/2\pi$ the average force between the dipole and the layer structure takes the form of an image force $\mathbf{F}_{\text{image}}$ given by

$$\mathbf{F}_{\text{image}}(z) = -\frac{\partial U_{\text{image}}}{\partial z}, \tag{24}$$

where U_{image} is the image potential. It is well-known that this potential arises as the change in the self-energy due to the presence of the layer structure, but it is also dependent on the average orientation of the electric dipole. It should be borne in mind that the evanscent field has no role to play in the determination of this potential, except that it is responsible for dipole orientation. The average dipole aligns itself parallel to $\hat{\mathbf{e}}$, a unit vector in the direction of the local evanescent electric field vector. This applies at every point along the trajectory.

The leading contribution to the image potential U_{image} is the instantaneous Coulomb interaction between the dipole and its image. We write

$$U_{\text{image}}(z) = -\frac{\mu^2}{32\pi\epsilon_0 z^3}\{3(\hat{\mathbf{e}}\cdot\hat{\mathbf{z}})(\tilde{\hat{\mathbf{e}}}\cdot\hat{\mathbf{z}}) - \hat{\mathbf{e}}\cdot\tilde{\hat{\mathbf{e}}}\}, \tag{25}$$

where $\tilde{\hat{\mathbf{e}}}$ is in the direction of the dipole image vector. In this image potential the addition of the metallic film has completely screened the effects of the dielectric substrate. There are clearly a number of approximations in adopting this potential. First the dipole motion would introduce velocity-dependent effects, but these are assumed to be small relative to the leading Coulomb potential given by Eq. (25). Second the image potential does not discriminate between the excited state and the ground state, while, in principle, the atom experiences different potentials in the two states. Third, the form of potential does not take into account fluctuation effects.

In terms of the average forces the reflection process is controlled by two separate mechanisms. First the spontaneous force $\mathbf{F}_s$ acts to accelerate (or decelerate) the atom in the direction of $\mathbf{k}_\parallel$ and, second, the combined force $\mathbf{F}_d + \mathbf{F}_{\text{image}}$ acts to repel the atom from the surface at a well-defined turning point in the trajectory. The average dipole potential U_d is such that $\mathbf{F}_d = -\partial U_d/\partial z$ with U_d having the well known form

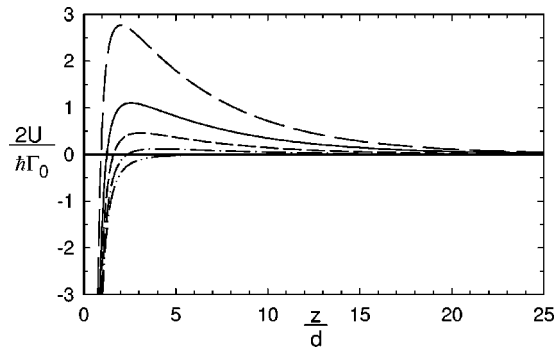

FIG. 4. Variation with z (in units of $d = 59$ nm) of the combined static dipole potential $U = U_d + U_{\text{image}}$ acting on a Rb atom (in units of $\hbar\Gamma_0/2$, with $\Gamma_0 = 6.128\times10^6$ s^{-1}). The static detuning is $\Delta_0 = 5.0\times10^2\ \Gamma_0$ and the arrangement is for an atomic mirror with a silver film of thickness $d = 59$ nm but different values of angle of incidence ϕ. They are as follows: $\phi = 42.10°$ (full curve); $\phi = 42.20°$ (long dashes); $\phi = 42.30°$ (short dashes); and $\phi = 42.40°$ (dash-dots). The dash-double dotted curve shows the variation of the van der Waals potential. In the evaluation of the potentials, the direction of the dipole moment vector conforms with the field-dipole orientation picture. The intensity of the incident light is taken as $I = 4\times10^2$ W m^{-2} for Rb at transition wavelength $\lambda_0 = 780$ nm.

$$U_d(z,\mathbf{v}) = \frac{\hbar\Delta(\mathbf{v})}{2}\ln\left[1 + \frac{2\Omega_R^2(z)}{\Delta^2(\mathbf{v}) + \Gamma^2}\right]. \tag{26}$$

The conventional derivation of average dipole force corresponding to Eq. (26) makes use of density matrix methods leading to the average forces given by Eq. (22) emerging in the steady state. However, these forces can also be derived using entirely classical arguments on the basis of a bound oscillator in external fields [23]. The same expressions were used in Refs. [18] and [19] in connection with the experimental results. We therefore adopt this form of the average dipole potential in our description of the operation of the atomic mirror with a metallic layer. A fuller description which allows a wide range of parameters such as detuning and field intensity and which incorporates fluctuations and spontaneous emission effects can be attained within the Monte Carlo approach, as discussed by Seifert *et al.* [24].

The total repulsive potential $U(z,\mathbf{v}) = U_{\text{image}}(z) + U_d(z,\mathbf{v})$ is shown in Fig. 4 for a typical set of parameters [18,19]. It should be noted that the field-dipole orientation picture influences the variations of both U_{image} and U_d. Since the potential profile depends on the angle of incidence ϕ, Fig. 4 displays potential profiles for a selection of angle of incidence and it is seen that for silver a resonance occurs around $\phi = 42.20°$.

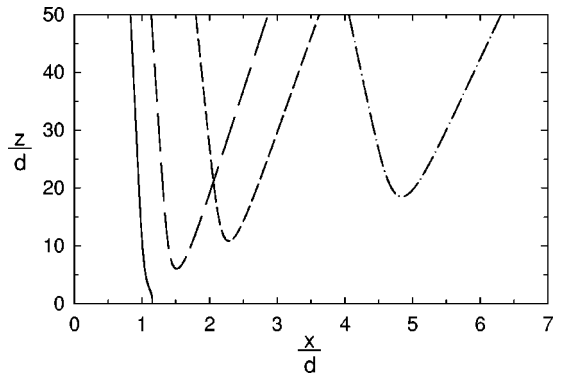

FIG. 5. Atomic trajectories of a Rb atom in the atomic mirror arrangement shown in Fig. 1 with a silver layer of width $d=59$ nm. The x-z plane is assumed to be the plane of incidence, with the angle of incidence of light fixed at $\phi=42.20°$. In all cases the initial position of the atom is at the point $(x=0,\ z=1000d)$. The different trajectories correspond to the same initial condition for the horizontal component of the velocity $v_{\parallel}(0)=0.054\ \mathrm{ms}^{-1}$, but differ in their initial z component of velocity $v_z(0)$. They are as follows: $v_z(0)=0.2\ \mathrm{ms}^{-1}$ (dash-dots); $v_z(0)=0.5\ \mathrm{ms}^{-1}$ (short dashes); $v_z(0)=0.8\ \mathrm{ms}^{-1}$ (long dashes); and $v_z(0)=1.1\ \mathrm{ms}^{-1}$ (full curve). The parameters are the same as those in Figs. 2 and 4.

The trajectory of the atom of mass M approaching a mirror in a given set up is obtainable by solving the equation of motion

$$M\frac{d^2\mathbf{r}}{dt^2}=\mathbf{F}_s+\mathbf{F}_d+\mathbf{F}_{\mathrm{image}}-Mg\hat{\mathbf{z}} \tag{27}$$

subject to given initial conditions. Figure 5 displays typical trajectories in the plane of incidence. The parameters are such that the spontaneous rate Γ is taken to be the free space value Γ_0. This is in fact a very good approximation in the trajectory region which is far from the metallic layer. The static detuning is taken to be $\Delta_0=5\times10^2\ \Gamma_0$. Finally the intensity of the light is assumed to be $I=4.0\times10^2\ \mathrm{W\,m}^{-2}$. The low intensity regime is an appropriate regime in the context of the atomic mirrors considered here. The saturation parameter in this case is $S=2\Omega_R^2/(\Delta^2+\Gamma^2)$ evaluated at the film surface. It is easy to check using the parameter values adopted here that the saturation parameter S is such that $S<1$, indicating that there is no need to adopt the dressed atom approach [25] appropriate for the high intensity regime $S>1$.

It can be seen in Fig. 5 that the structure operates as an atomic mirror in three of the cases displayed, while for the fourth case the trajectory of the atom terminates with a collision at the surface. An approximate guide to the condition leading to a collision with the surface is to compare the maximum height $U_{\max}$ of the potential in Fig. 4 to the initial kinetic energy $Mv_z^2(0)/2$. For $v_z(0)>\sqrt{2U_{max}/M}$ a collision occurs. This interpretation indeed conforms with the results of the type shown in Fig. 5. Note that the reflected atom trajectories are, in general, asymmetric with respect to the turning point. This is a consequence of the action of $\mathbf{F}_s$ which in the present example where the light and the atom are incident on the same side (left side) of the z axis, accelerates the atom to the right along the surface. In principle, an optimization of the mirror parameters can be carried out for specific purposes to achieve predetermined trajectories and in such a manner as to avoid surface collisions.

V. COMMENTS AND CONCLUSIONS

Our main aim here was the construction of a theory of evanescent mode atomic mirrors with a metallic layer. We have shown that this theory has the advantage of being capable of providing information about the range of layer widths, metallic electron densities, and the angle of incidence at which the Rabi frequency and, hence, the repulsive potential, exhibits pronounced enhancement effects. Our results clearly indicate that enhancement is indeed possible and we have also quantified the operation of the mirror, deriving the trajectories for typical situations and thus demonstrated the mirror action.

An interesting limit of the theory is obtainable when the thickness of the metallic film becomes so small that it can be regarded as forming a metallic sheet. This metallic sheet limit is characterized by a finite areal electron density n_s defined by

$$n_s=\lim_{d\to0} n_0 d. \tag{28}$$

Application of the limit $d\to0$ (at fixed n_0) to the function ξ, as defined in Eq. (13), gives

$$\xi\to1+i\frac{k_{z2}\epsilon_1}{k_{z1}\epsilon_2}\left(\frac{\Lambda^2 k_{z1}L_0}{\omega^2}-1\right), \tag{29}$$

where we have set $\gamma=0$; Λ is a scaling frequency

$$\Lambda^2=\frac{n_s e^2}{m^*\epsilon_0\epsilon_1 L_0} \tag{30}$$

with L_0 a scaling length. Note that this limit is not the same as $d\to0$ in Fig. 3. Corresponding to the limit of ξ are reflectivity and Rabi frequency expressions, as defined in Eqs. (16) and (21), respectively. It can be checked that enhancement occurs when the Rabi frequency is a maximum, which amounts to a minimum of $|\xi|^2$ in the denominator of Eq. (21), with ξ given by Eq. (29). In fact maximum enhancement occurs when $|\xi|^2=1$ such that

$$\omega^2=\left(\frac{n_s e^2}{m^*\epsilon_0\epsilon_1}\right)k_{z1}. \tag{31}$$

The wave vector dependence makes this similar to (not the same as) the dispersion relation of surface modes supported by a metallic sheet [26–28]. For a finite film thickness a rough estimate of the metallic density n_0^{ϕ} is

$$n_0^{\phi}=\frac{c\omega m^*\epsilon_0\epsilon_1}{e^2 d[\epsilon_2\sin^2\phi-\epsilon_1]^{1/2}} \tag{32}$$

provided that $\epsilon_2 \sin^2\phi \neq \epsilon_1$. The simple result in Eq. (32) provides a guide for the metallic densities at which enhancement occurs, provided that the metallic film thickness is not too large.

ACKNOWLEDGMENTS

C.R.B. and J.B.K. are grateful to the EPSRC for financial support. This work has been carried out under the EPSRC Grant No. GR/M16313.

[1] V. I. Cooke and R. K. Hill, Opt. Commun. **43**, 258 (1982).
[2] V. I. Balykin, Adv. At., Mol., Opt. Phys. **4**, 181 (1999).
[3] J. P. Dowling and J. Gea-Banacloche, Adv. At., Mol., Opt. Phys. **37**, 1 (1997).
[4] R. J. Wilson, B. Holst, and W. Allison, Rev. Sci. Instrum. **70**, 2960 (1999).
[5] D. C. Lau, A. I. Sidrov, G. I. Opat, R. J. McLean, W. J. Rowlands, and P. Hannaford, Eur. Phys. J. D **5**, 193 (1999).
[6] C. V. Saba, P. A. Barton, M. G. Boshier, I. G. Hughes, P. Rosenbusch, P. E. Sauer, and E. A. Hinds, Phys. Rev. Lett. **82**, 468 (1999).
[7] R. Cote, B. Segev, and M. G. Raizen, Phys. Rev. A **58**, 3999 (1998).
[8] L. Santos and L. Roso, Phys. Rev. A **58**, 2407 (1998).
[9] N. Friedman, R. Ozeri, and N. Davidson, J. Opt. Soc. Am. **15**, 1749 (1998).
[10] P. Szriftgiser, D. Guery-Odelin, P. Desbiolles, J. Dalibard, M. Arndt, and A. Steane, Acta Phys. Pol. **93**, 197 (1998).
[11] L. Santos and L. Roso, J. Phys. B **30**, 5169 (1997).
[12] A. Landragin, J. Y. Courtois, G. Labeyrie, N. Vansteenkiste, C. I. Westbrook, and A. Aspect, Phys. Rev. Lett. **77**, 1464 (1996).
[13] N. Vansteenkiste, A. Landragin, G. Labeyrie, R. Kaiser, C. I. Westbrook, and A. Aspect, Ann. Phys. (Paris) **20**, 595 (1995).
[14] A. Landragin, G. Labeyrie, J. Y. Courtois, R. Kaiser, N. Vansteenkiste, C. I. Westbrook, and A. Aspect, Ann. Phys. (Paris) **20**, 641 (1995).
[15] G. Labeyrie, A. Landragin, J. VonZanthier, R. Kaiser, N. Vansteenkiste, C. I. Westbrook, and A. Aspect, Quantum Semiclassic. Opt. **8**, 603 (1996).
[16] N. Vansteenkiste, R. Kaiser, Y. Levy, A. Aspect, W. Seifert, D. Leipold, and J. Mlynek, Ann. Phys. (Paris) **20**, 129 (1995).
[17] S. M. Tan and D. F. Walls, Phys. Rev. A **50**, 1561 (1994).
[18] S. Feron, J. Reinhardt, S. Lebouteux, O. Gocreix, J. Baudon, M. Ducloy, J. Robert, C. Miniatura, S. N. Chormaic, H. Haberland, and V. Lorent, Opt. Commun. **102**, 83 (1993).
[19] T. Esslinger, M. Weidenmüller, A. Hammerich, and T. W. Hänch, Opt. Lett. **18**, 450 (1993).
[20] R. Loudon, *The Quantum Theory of Light*, 2nd ed. (Oxford, Uiversity, New York, 1995).
[21] M. Babiker and S. Al-Awfi, Opt. Commun. **168**, 145 (1999).
[22] L. Allen, M. Babiker, W. K. Lai, and V. E. Lembessis, Phys. Rev. A **54**, 4259 (1996).
[23] S. C. Zilio and V. S. Bgnato, Am. J. Phys. **57**, 471 (1989).
[24] W. Seifert, C. S. Adams, V. I. Balykin, C. Heine, Yu Ovchinnikov, and J. Mlynek, Phys. Rev. A **49**, 3814 (1994).
[25] J. Dalibard and C. Cohen-Tannoudji, J. Phys. B **18**, 1661 (1985).
[26] F. Stern, Phys. Rev. Lett. **18**, 546 (1967).
[27] A. L. Fetter, Ann. Phys. (N.Y.) **81**, 367 (1973).
[28] C. R. Bennett, J. B. Kirk, and M. Babiker (unpublished).